Research Article

Journal of Environmental Nanotechnology

Laboratory Investigation of Nanofluid-filled Wickless Heat Pipes for a Parabolic Dish Solar Heat Collector

Harendra Kumar Jha* and Arun Kumar
Department of Mechanical Engineering, NIT, Patna, India
Received: 10.01.2026 Accepted: 27.02.2026 Published: 30.03.2026
*harendraj.phd19.me@nitp.ac.in

ABSTRACT

Solar thermal conversion was achieved by preparing a nanofluid using ethanol and acetone as base fluids and Cu nanoparticles of optimized size (~20 nm) as the additives. The thermophysical properties of the nanofluid were determined at different temperatures, and their temperature-dependent variations were analyzed to assess their potential to enhance the thermal efficiency of wickless heat pipes. The performance of the wickless heat pipe filled with ethanol and acetone as base fluids was evaluated by measuring the heat input and output at the inlet and outlet. Both ethanol and acetone exhibited an optimized filling ratio of 40%. The overall thermal efficiency was then determined, and the efficiency and overall thermal resistance were compared between ethanol- and acetone-filled heat pipes, accounting for radiation-induced heat input over a one-hour daytime interval. Based on the calculations, the minimum and maximum thermal efficiencies were found between the range of 42.30% to 58.48% for Cu-Acetone based nanofluid and for Cu-Ethanol-based nanofluid it was found between the range of 37.83% to 54.01%, which was 4.47% lower than that of Cu- Acetone based nanofluid .The overall thermal resistance was determined to be 0.076 °C/W for the acetone heat pipe and 0.074 °C/W for the ethanol heat pipe.

Keywords: Parabolic dish solar heat collector; Nanofluids; Wickless heat pipe; Acetone; Ethanol.

1. INTRODUCTION

Heat pipes are effective heat transfer devices. They use principles of fluid evaporation and condensation. They are comprised of a sealed copper or aluminum pipe, a small amount of operating fluid, and an interior wick structure. The operating fluid at the evaporator section of the heat transfer pipe is heated by the heat source. The parabolic solar ray collector turns the liquid into vapour. Due to their distinct thermal and rheological characteristics, nanofluids offer a lot of potential in a variety of sectors. Nanofluids have the potential to boost the heat transfer coefficients of solar water heaters and the thermal efficiency of storage devices. This is due to an increase in absorption of solar light by nanoparticles. Heat is transferred when the vapour flows towards the cold condenser section of the heat pipe. In condensation, the heat escapes to the heat sink (such as a storage tank or heat exchanger) as the vapour condenses on the inside surfaces of the condenser section. In the capillary action cycle, the condensed fluid is returned to the evaporating portion employing the capillary motion. High thermal efficiency, low resistance to heating, and the capacity of transferring heat over long distances with little energy input are just a few benefits offered by heat pipes.

Using a parabolic-shaped mirror reflector, a parabolic solar collector directs sunlight onto a focal point. The evaporator section of the heat pipe receives the concentrated solar radiation focused by the parabolic dish solar collector. The appropriate working fluid is selected based on its compatibility with the heat pipe material and its vaporization characteristics. Ammonia, water, and other refrigerants are some of the commonly used working fluids. The integrated system undergoes a series of tests to evaluate its thermal efficiency and identify potential areas for improvement. This may involve modifying design parameters such as the size and shape of the parabolic reflector or the characteristics of the heat pipe.

Mohammed *et al.* (2022) demonstrated that integrating a heat pipe with a solar collector significantly enhances heat transfer efficiency, improves performance stability under varying weather conditions, and enables the production of higher-temperature water compared to a conventional solar thermal collector system. Shady *et al*. (2022) investigated the effect of using a hybrid magnesium oxide–multi-walled carbon nanotube (MgO/MWCNT) nanofluid on the thermal performance of a vacuum-sealed tube solar receiver. For MgO/MWCNT on a water basis, four distinct weight ratios of (80:20), (70:30), (60:40), and (50:50) were used, respectively. The weight ratio of 50:50 performed better than any other mixture of nanofluids and was closer to the MWCNT/water nanofluid. Tardy and Sami (2009) noticed a rise in the net heat flux of the nanofluid employed in the heat pipe as well as its thermal behaviour. It was found that when CuO composition is higher, thermal energy is more directed to the heat pipe's evaporator portion, which boosts the system's hybrid

system efficiency. Sinan *et al.* (2021) found that aluminium oxide with water and titanium oxide with water can increase the thermal efficiency of heat pipe solar collectors. When applying pure water as a base fluid, the greatest value of instantaneous point efficiency was calculated to be 48%; for aluminium oxide and water nanofluid, it is 58%; and for titanium oxide and water nanofluid, it is 64%. Al_2O_3 and water nanofluids were found to have an efficiency improvement of 20.8%, whereas TiO_2 and water nanofluids had an improvement of 33.3%. Mohammad *et al*. (2019) reviewed the results of utilizing several nanofluids in heat pipes. When compared to water-filled heat pipes, it has been found that employing graphene oxide/water nanofluid in pulsing heat pipes can lower thermal resistance by up to 42%. Leonard *et al*. (2017) worked on the thermal performance of heat pipes using nanofluids. Past works on the use of nanofluids in different heat pipes were reviewed. Al_2O_3, CuO, and TiO_2 were found to have the greatest reductions in total thermal resistance of 83%, 79%, and 76%, respectively. Sabiha *et al.* (2015) worked on the energy performance of a vacuum-sealed tube solar collector using a walled carbon nanotube. In the observation, collector efficiency was found to be 71.84% higher than that of water. The heating capacity of a cylindrical heat conduit using nanofluids was investigated in two dimensions by Shafahi *et al.* (2010). Three of the most used nanoparticles, namely Al_2O_3, CuO, and TiO_2, are considered for standard studies. The nanoparticles in the liquid boosted the heat pipe's thermal performance by minimizing its thermal resistance while raising the amount of heat it can transport. It was observed that the thermal efficiency of the heat pipe is affected by particle size; the smaller particles will have a more noticeable impact on the heat pipe's temperature distribution. For Pise *et al*. (2016), the primary objective of the study was to examine the thermal performance of a heat pipe with a parabolic solar receiver under actual working circumstances. Distilled water, Al_2O_3–water nanofluids with varying weight concentrations (0.05, 0.25, and 0.5 wt.%), Al_2O_3–water nanofluid with a surfactant, and water with a surfactant were employed as working fluids. It was observed that the collector efficiency increased with coolant flow rate up to an optimum value and then decreased. The tilt angle follows a similar trend and reaches its maximum at 50 degrees. Gan *et al.* (2018), for improving the heat transport properties of a heat pipe, applied three alternative heat loads and cooling water mass flow rates to the evaporator and condenser sections, respectively, and examined experimentally and numerically. Deionized water and aqueous clinoptilolite nanofluid heat pipe efficiency and thermal resistance values were evaluated. Ali *et al*. (2018) emphasized that maintaining thermal and physical properties over long periods after preparation requires high nanofluid stability. Enhancing nanofluid stability and comprehending nanofluid behaviour are, therefore, essential steps in the chain required to commercialize this kind of sophisticated fluid. The article's goal is to review the most recent developments in the examination of small-sized matter, including Manufacturing techniques, stability enhancement mechanisms, stability augmentation techniques, thermophysical characteristics, and current commercialization hurdles. Xuan and Li (2000) worked on heat transfer enhancement of nanofluids. Ghadimi *et al.* (2011) reviewed the stability characteristics and characterization of nanofluids under stationary settings, illustrating the generic stabilization techniques as well as distinct stability inspection devices. After preparation using a one-step or two-step process, nanofluid characterization, analytical models, and measurement techniques were examined (Vand *et al*. 2009). Carbon nanotubes were used, and their surfaces were covalently modified to stabilize nanofluid suspensions (Teng *et al*. 2010). In this study, the heating capacity ratio of alumina (Al_2O_3)/water-based nanofluids was examined with respect to weight, temperature, and nanoparticle size. In this experiment, the thermal conductivity of nanofluids running at temperatures of 10 °C, 30 °C, and 50 °C with a range of particle sizes and weight fractions was determined. Choudhary *et al.* (2017) carried out a stability analysis of the Al_2O_3/water nanofluid. Visual examination techniques and zeta potential approaches were used to investigate the stability. In-depth research was done on how pH and sonication time affect the stability of nanofluids. The stability period of nanofluids was determined using the visual examination approach. The stability period of nanofluids was directly correlated with the zeta potential; the longer the absolute value of the zeta potential, the longer the stability period. Sodium dodecyl sulphate, a surfactant, was used to examine the stability with respect to the time duration since the creation of nanofluids. Xu *et al.* (2017) made an experimental assessment of a solar collector that combines a compound parabolic concentrator (CPC) and a closed-end pulsing heat pipe (PHP). Because of its simple design and substantial capability for heat transfer, PHP was employed as an absorber. Experimental research was done on the thermal efficiency and operating features of the solar collector. The PHP absorber's evaporation and condensation sections' regular and constant temperature changes showed that it can operate effectively with a thermal resistance of roughly 0.26 °C/W. Additionally, it was discovered that being the primary contributor to the collector's thermal performance of the PHP absorber diminishes with rising evaporation temperatures. Yang *et al.* (2008) used CuO nanofluid as the working fluid to examine the heat transfer capabilities of a horizontal micro-sized grooved heat pipe. A consistent suspension of deionized water and CuO nanoparticles was known as CuO nanofluid. The critical heat flux and the overall heat resistance of the heat pipe, as well as the effects of the mass concentration of CuO nanoparticles, were discussed. The heat pipe's thermal performance can be augmented by using CuO nanofluid, according to experimental data. The best mass concentration for this purpose is anticipated to be 1.0 wt.%. Chen *et al*. (2008)

used a flat-shaped heat pipe with a silver nano-fluid. By using air-cooling testing equipment, they examined how different concentrations affect the thermal performance of flat heat pipes. Silver particles measuring 35 nm in size were used in these tests. Water was the basic operating fluid. To assess the temperature distribution of the heat pipe and determine the thermal resistance, an experimental apparatus was set up by Choi *et al*. (1995). The possible benefits of the fluids were estimated, and it was shown that a significant decrease in heat exchanger pumping power was one of the major benefits of nanofluids.

In recent years, nanofluids have attracted more attention. The main driving force for research on nanofluids lies in their wide range of applications. Most of the reviews are concerned with the experimental and theoretical studies of the thermophysical properties or the convective heat transfer of nanofluids. The purpose of this work is to focus on the new methods and stability mechanisms.

In the two-phase heat transfer device technique, nanofluids give better results. Some of the researchers worked on the effective enhancement of heat transfer by using a wickless heat pipe with different nanofluids and inclination angles. This work is a detailed study of parabolic dish-type solar water heating systems by using two thermosyphons filled with nanofluids (ethanol and acetone with Cu nanoparticles) as a heat transfer tool for an energy storage system.



Fig. 1: Actual test setup

2. EXPERIMENTAL SECTION

Solar water heating systems are typically of two types: flat-plate collectors and evacuated tube water heaters. Recently, some researchers have started exploring parabolic dish and trough-type solar collectors for water heating applications. However, due to limitations in design and insufficient data analysis, parabolic dish-type domestic water heaters have not yet demonstrated effective enhancement of solar heat transfer. The proposed research aims to develop a rooftop parabolic dish-type water heater with effective solar heat transfer performance. Literature review indicates that optimizing heat transfer and energy utilization through careful parameter selection is significant for improving water heater efficiency. In conventional systems, a large portion of incident solar radiation remains unabsorbed, and significant heat losses to the atmosphere further reduce energy efficiency, often resulting in values lower than expected. The important components are parabolic shape reflectors (mirrors) that concentrate sunlight at the focal area. Two wickless heat pipes are used to transfer the absorbed heat from the focal point to an insulated cold-water storage tank, as shown in Fig. 1

2.1 Design Considerations

All the parts used in dish-type water heaters are required to have a certain engineering measure to be considered suitable for both built-up and domestic use. A simple method for constructing a parabolic dish is to cut and fold sheet metal into the desired parabolic shape, as shown in Fig. 1. The inner surface can then be covered with mirror fragments to reflect incoming solar rays toward the focal point. A mild steel sheet of size 24 sq. ft. (6 ft. × 4 ft.) was used for the parabolic reflector. The parabolic base was made with mild steel strips of 7 mm width. Mild steel angle iron of 12 mm width and nut bolts were used for frame rotation. Fragments of glass in a rhombus shape were used for the reflector. Silica gum was used to stick the mirrors to the total inner surface area of the parabolic solar concentrators. The dual laser pyrometer was used to measure the temperatures at the focus. For effective implementation, the mechanical design of a solar heat accumulator or concentrator must ensure safety, reliability, and ease of use in domestic heating applications.

2.2 Nanofluid Preparation

Fig. 2 illustrates the weighing method for nanoparticles, in which particles approximately 20 nm in size are dispersed for nanofluid applications to achieve good dispersion. Surfactants are occasionally employed to enhance nanofluid stability. In addition, surface modification of the dispersed nanoparticles and the application of strong forces to break up agglomerates may improve the durability of the particles in the base fluid. Nanofluids can be prepared using one-step or two-step physical methods. Another advanced approach for producing nanofluids involves chemical synthesis.

2.3 Sonication

The sonication method (Fig. 3) improves the dispersion mechanism, which reduces the probability of particle clustering compared with the magnetic stirring method. In this technique, ultrasonic waves are transmitted through the nanofluid. Sonication facilitates the formation of a more uniform composite suspension.

There are two distinct sonication methods: probe type and bath type. Probe sonication generally yields better results than bath sonication.

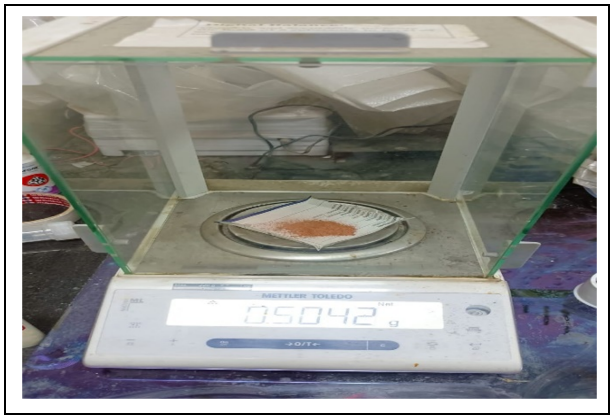


Fig. 2: Weighing of nanoparticles

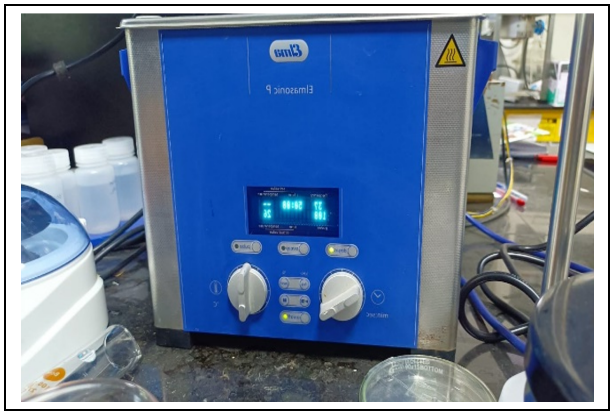


Fig. 3: Sonication of nanofluid

2.4 Magnetic Stirring

A magnetic stirrer, also called a magnetic mixer, is a laboratory tool that stirs or mixes liquids using a rotating magnetic field (Fig. 4). A tiny bar magnet is inserted into the liquid to be stirred, and a magnetic stir plate is positioned beneath the liquid container. When the stir plate is activated, the magnetic field rotates the bar magnet, stirring the liquid as a result. Some magnetic stirrers feature a built-in heating element in addition to stirring, allowing the temperature of the liquid to be controlled. The heating element and liquid temperature are normally controlled by moving the correct knob on a magnetic stirrer.

2.5 Enhancing Nanofluid Stability

Dispersants or surfactants are frequently added to nanofluids to increase stability, which avoids nanoparticle agglomeration by lowering the surface tension of the operating fluid. However, excessive usage of the dispersant can harm the thermal properties and physical characteristics (reduction in heat-conducting ability and chemical stability). Hence, the dispersant should be used in the appropriate amount. Sodium dodecyl benzene sulfonate (SDBS), gum arabic, sodium dodecyl sulphate, polyvinyl pyrrolidone, dodecyl trimethyl ammonium bromide, oleic acid, and others are examples of common dispersants. Additionally, surfactants such as Disponil, Hypermer, and Aerosol are used.

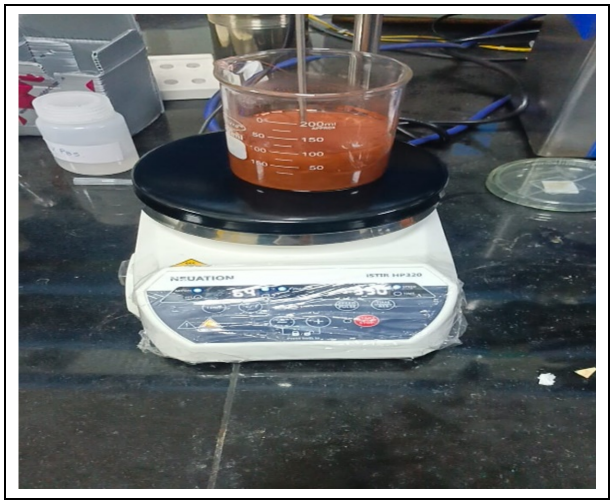


Fig. 4: Magnetic stirring of nanofluid

2.6 Evaluation of Nanofluid Stability Through Zeta Potential

The zeta potential is the potential difference between the stationary fluid layer adhering to nanoparticles and the bulk fluid. Ghadimi *et al.* (2011) reported that lower zeta potential nanofluids exhibited faster deposition of tiny particles (about 100 nm) throughout the standard fluid, whereas a higher magnitude of zeta potential (positive or negative) portrays the electrically steady suspended solution. Vand (2009) suggested that nanofluids are moderately stable when the zeta potential is around 30 mV and are considered to have good stability when it approaches 45 mV.

2.7 Effect of Surfactant

The impact of surfactants on the zeta potential of copper in an ethanol-based nanofluid was studied at a composition of 0.01 vol.%. SDBS was added to the nanofluid before sonication, and the zeta potential was monitored over time (in days). Surfactants have a head and tail and resemble a chain. The negative functional group is on the tail side of the anionic surfactants, while the positive functional group is on the head side. The nanoparticles are drawn to the positive head, which then binds to them. As a result, the tail-negative charge in the electrically laminated layer grows, augmenting the zeta potential's (negative) magnitude. Zeta potential measurements range from 30 to 26 mV.

3. ANALYSIS AND CALCULATIONS

3.1 Calculation of Density and Viscosity

W_1 = weight of pycnometer

W_2 = weight of pycnometer along with ethanol (base fluid)

W_3 = weight of pycnometer along with nanofluid having the same volume as that of ethanol

ρ_1 = density of base fluid (ethanol)

ρ_2 = density of nanofluid

T_1 = mean time of base fluid

T_2 = mean time of nanofluid

μ_1 =Viscosity of base fluid at room temperature

μ_2 =Viscosity of nanofluid

$$\rho_2=\frac{W3-W1}{W2-W1} \quad \ldots (1)$$

$$\mu_2 = \frac{\rho 2\times T2}{\rho 1\times T1}\times \mu 1 \quad \ldots (2)$$

W_1 = 12.97 g

W_2 = 20.162 g

W_3 = 20.6375gm

$$\rho_2 = \frac{w_3-w_1}{w_2-\omega_1} = \frac{20.6375-12.97}{20.162-12.97} = 0.9996 g/cm^3$$

$$\mu_2 = \frac{\rho 2\times T2}{\rho 1\times T1}\times \mu 1 = \frac{0.9966\times 22033}{0.7849\times 2.166}\times 1.1 = 1.4073 \text{ cP}$$



Fig. 5: Viscosity measurement using a viscous calorimeter



Fig. 6: Water bath treatment

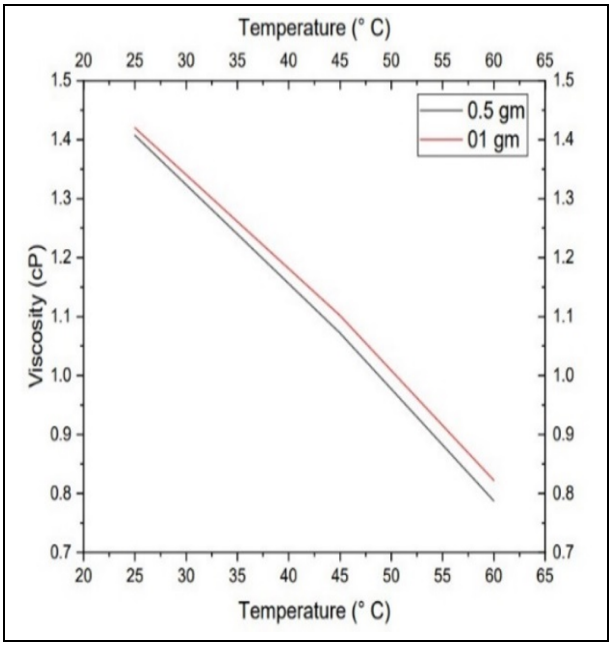


Fig. 7: Temperature *vs.* viscosity graph for 100 mL of base fluids

3.2 Thermophysical Properties of Nanofluid

3.2.1 Volume Concentration

$$\text{Volume concentration, } \boldsymbol{\phi} = \frac{\frac{w_{np}}{p_{np}}}{\frac{w_{np}}{p_{np}}+\frac{w_{bf}}{P_{bf}}} \quad \ldots (3)$$

where, W_{np} is the weight of nanoparticles, P_{np} is the density of nanoparticles, W_{bf} is the weight of standard fluid, and P_{bf} is the density of standard fluid.

3.2.2 Density of Nanofluid

For nanofluids, the density is estimated using the standard mixture law. According to the composition law, the density of a nanofluid can be expressed as,

$$P_{n_f} = P_{n_P}\phi + P_{bf}(1-\phi) \quad \ldots (4),$$

where, P_{nf} is the nanofluid density, P_{n_P} is the nanoparticle density, P_{bf} is the base fluid density, and ϕ is the nanoparticle volume fraction.

3.2.3 Specific Heat of Nanofluid

The specific heat of nanofluids can be evaluated using the mixture law:

$$C_{Pn_f} = C_{Pn_P}\phi + C_{P_{nf}}(1-\phi) \quad \ldots (5)$$

where, C_{pnf}, C_{pnp}, and C_{pbf} are the specific heats of the nanofluid, the nanoparticles, and the base fluid, respectively, and ϕ is the nanoparticle volume fraction.

3.2.4 Thermal Conductivity of Nanofluid

Using Maxwell's equations, we can find out the thermal conductivity of the nanofluid.

$$\frac{k_{nf}}{k_{bf}} = \frac{k_p + 2k_{bf} + 2\phi(k_p - k_{bf})}{k_p + 2k_{bf} - \phi(k_p - k_{bf})}$$

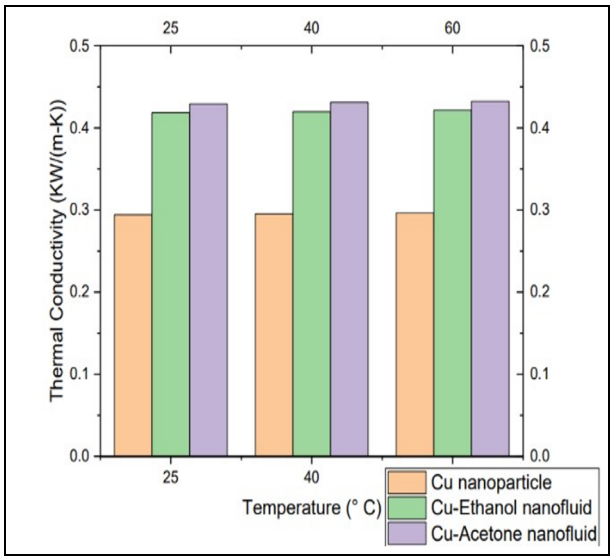


Fig. 8: Temperature *vs.* thermal conductivity graph for 100 mL of the base fluids

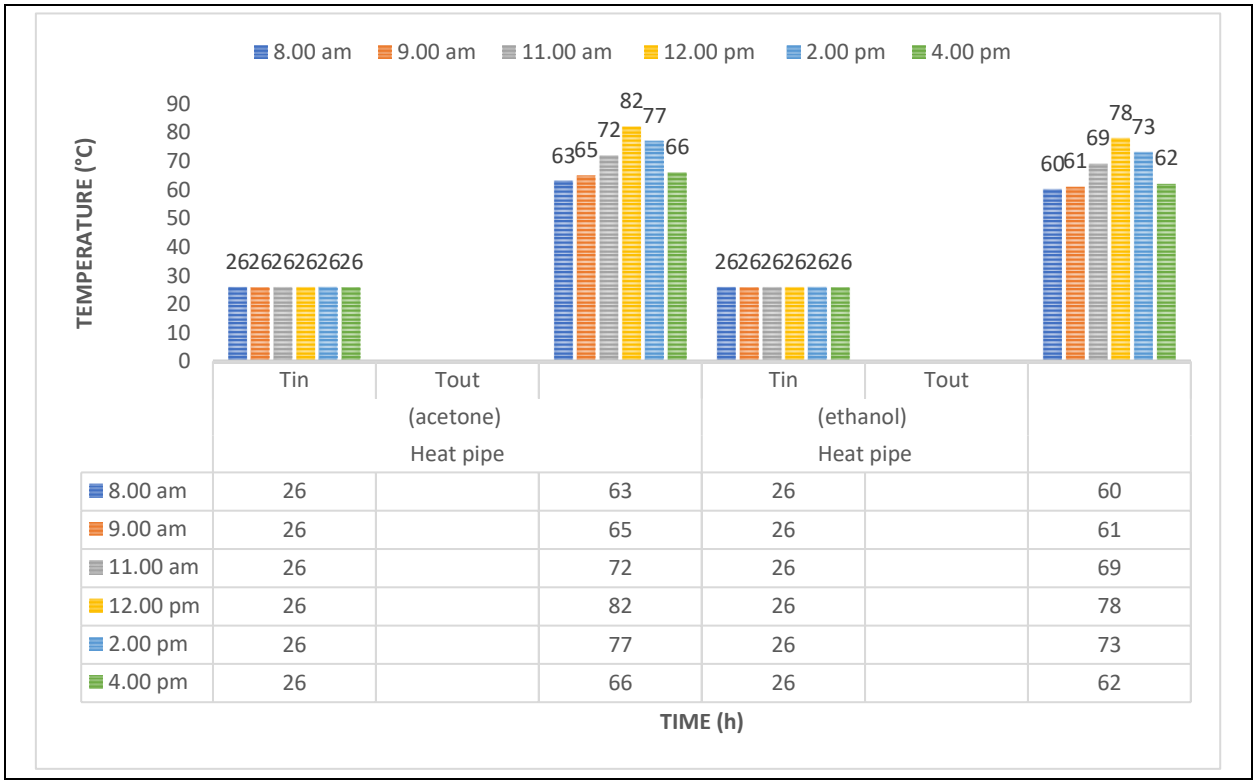
4. RESULTS AND DISCUSSION

The cooling water flowing through the water jacket absorbs the latent heat of vaporization from the vapour generated in the evaporator section. As a result, the vapour condenses back to liquid and, through the capillary action of the wick, returns to the evaporator section. Fig. 9 shows the inlet and outlet temperatures of the cooling liquid when ethanol and acetone are used as base fluids in the heat pipe. The outlet temperature of acetone is higher than that of ethanol. This behavior can be attributed primarily to the lower specific heat capacity of acetone, which results in a greater temperature rise for the same heat input and consequently a higher exit temperature of the coolant.

As the tilt angle of the heat pipe increases, the mass flow rate rises and reaches its optimum value at 45°. Beyond this angle, the mass flow rate decreases, attaining its minimum value when the pipe is positioned vertically. This behavior is primarily influenced by gravitational effects. Fig. 10 shows the comparative heat input performance with time for both the ethanol- and acetone-filled heat pipes. Fig.11 shows that as the heat input increases around 1:00 pm, the efficiency reaches its maximum; as the heat input decreases, the efficiency of the heat pipe correspondingly declines. The maximum efficiency of the acetone-filled heat pipe at a tilt angle of 60° was 55.46%, which is 0.813% lower than that at a tilt angle of 45°. Figures 12 and 13 show the efficiency for ethanol- and acetone-filled heat pipes at different angles, respectively. The optimum tilt angle for the maximum thermal efficiency of a heat pipe is 45°. The efficiency increases till the tilt angle reaches 45°, and beyond that, it starts decreasing due to reduced mass flow rate and gravitational effect.

Fig. 15 shows the variation of efficiency with different tilt angles of the heat pipe for both acetone and ethanol. It was noted that the heat pipe efficiency for the acetone-filled pipe was higher than that of the ethanol-filled heat pipe, as the specific heat capacity of acetone is lower than that of ethanol. This is because there is a temperature difference between the acetone vapour and cooling liquid, which facilitates heat rejection, and as a result heat transfer efficiency of the heat pipe is higher. The filling ratio of 40% was considered for both acetone and ethanol fluids. The minimum and maximum thermal efficiencies found between the range from 42.30% to 58.48% for Cu-Acetone based nanofluid and ranges between 37.83% to 54.01% for Cu-Ethanol based nanofluid, which was 4.47 % lower than that for Cu-Acetone based nanofluid.

Fig. 16 illustrates that with increase in the tilt angle; the solar intensity decreases. This is because when the tilt angle increases, the path length for sun rays also increases. Dust and other suspended particles scatter light that causes the solar intensity to decrease.



	Tin	Tout	(acetone) Heat pipe	Tin	Tout	(ethanol) Heat pipe
8.00 am	26		63	26		60
9.00 am	26		65	26		61
11.00 am	26		72	26		69
12.00 pm	26		82	26		78
2.00 pm	26		77	26		73
4.00 pm	26		66	26		62

Fig. 9: Temperature vs. time graph of the heat pipes

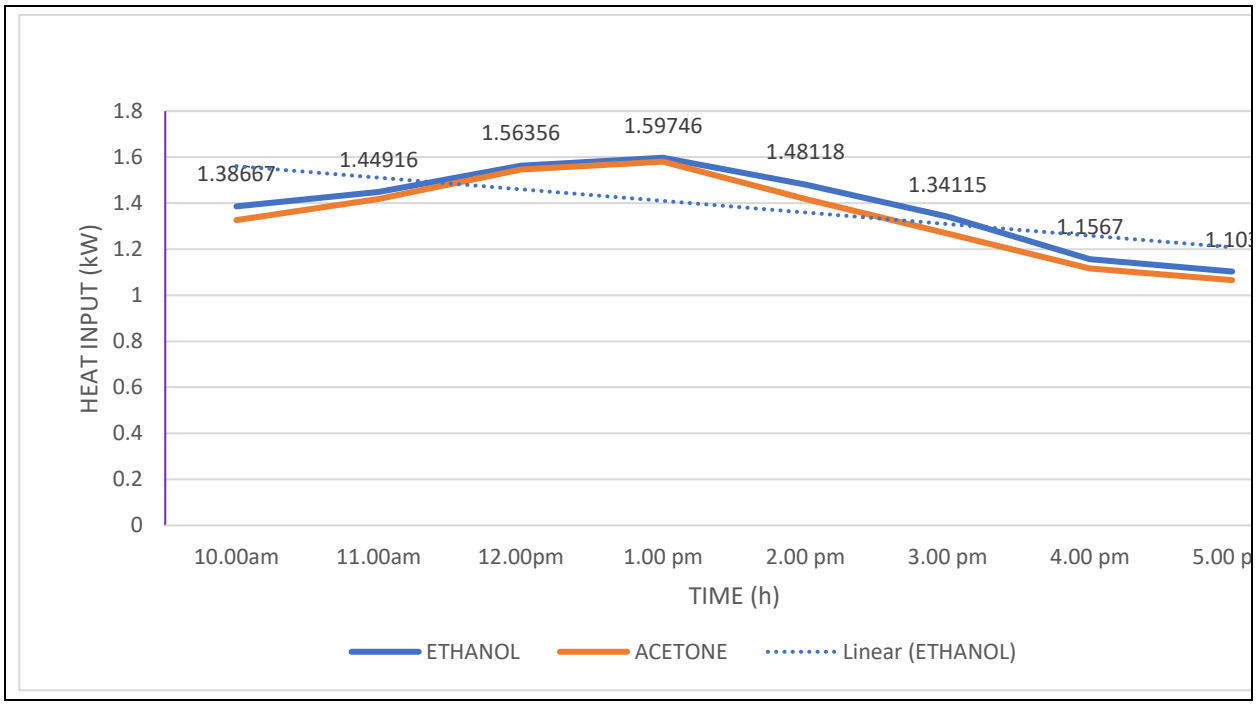
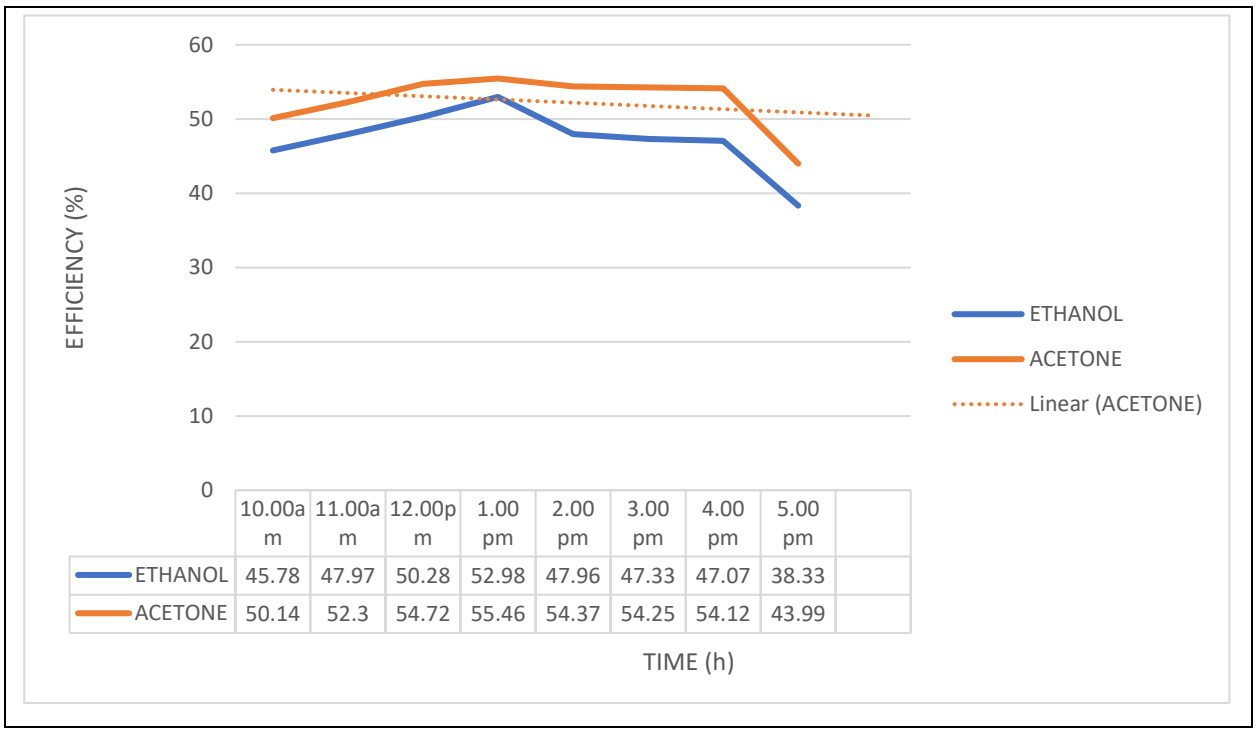


Fig. 10: Heat input *vs.* time plot for ethanol- and acetone-filled heat pipes



	10.00am	11.00am	12.00pm	1.00 pm	2.00 pm	3.00 pm	4.00 pm	5.00 pm
ETHANOL	45.78	47.97	50.28	52.98	47.96	47.33	47.07	38.33
ACETONE	50.14	52.3	54.72	55.46	54.37	54.25	54.12	43.99

Fig. 11: Variation of heat pipe efficiency with time for ethanol- and acetone-filled heat pipes

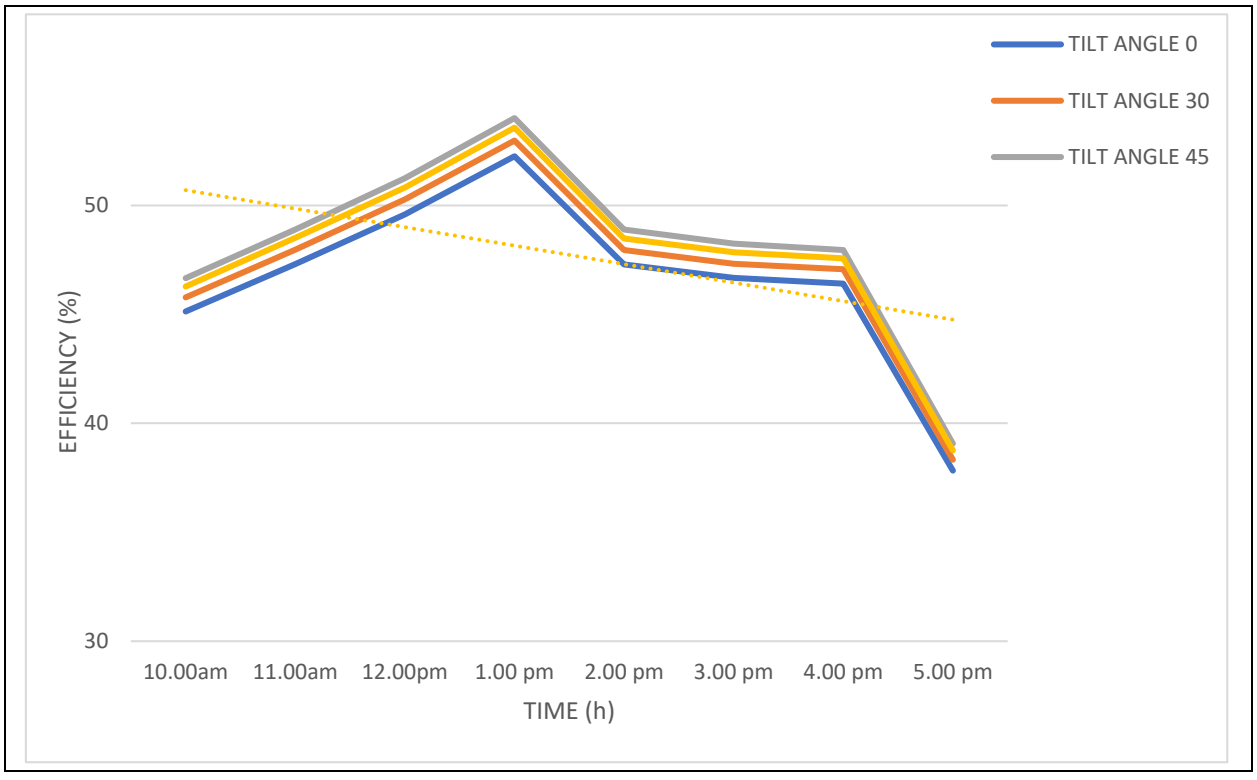
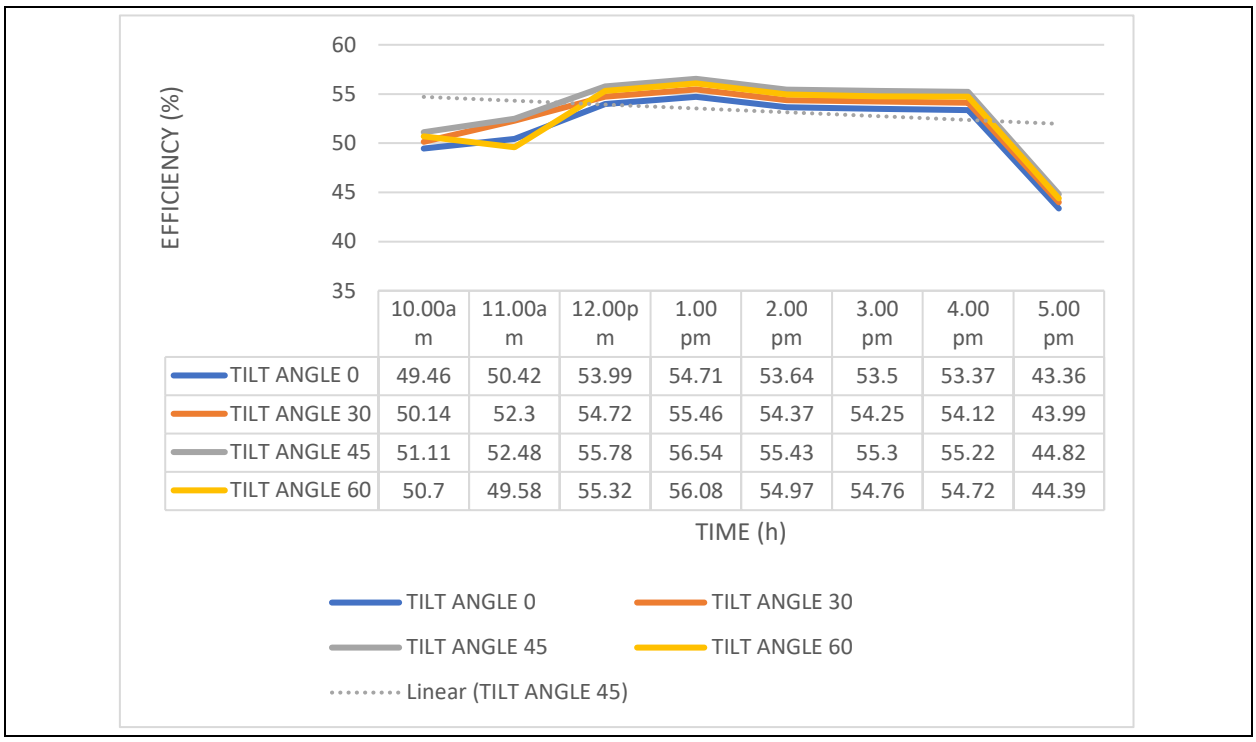
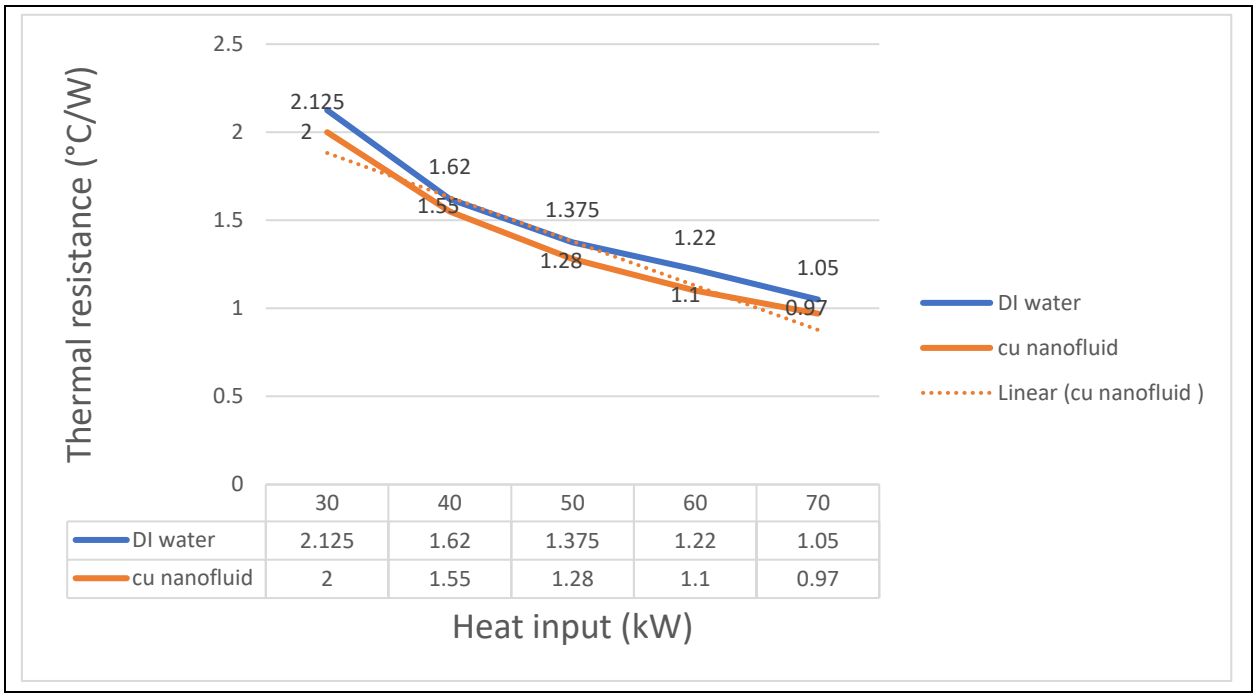


Fig. 12: Heat pipe efficiency *vs.* time for ethanol-filled heat pipe at different tilt angles



	10.00am	11.00am	12.00pm	1.00 pm	2.00 pm	3.00 pm	4.00 pm	5.00 pm
TILT ANGLE 0	49.46	50.42	53.99	54.71	53.64	53.5	53.37	43.36
TILT ANGLE 30	50.14	52.3	54.72	55.46	54.37	54.25	54.12	43.99
TILT ANGLE 45	51.11	52.48	55.78	56.54	55.43	55.3	55.22	44.82
TILT ANGLE 60	50.7	49.58	55.32	56.08	54.97	54.76	54.72	44.39

Fig. 13: Heat pipe efficiency *vs.* time plot for acetone-filled heat pipe at different tilt angles



	30	40	50	60	70
DI water	2.125	1.62	1.375	1.22	1.05
cu nanofluid	2	1.55	1.28	1.1	0.97

Fig. 14: Thermal resistance *vs.* heat input for DI water and Cu nanofluid

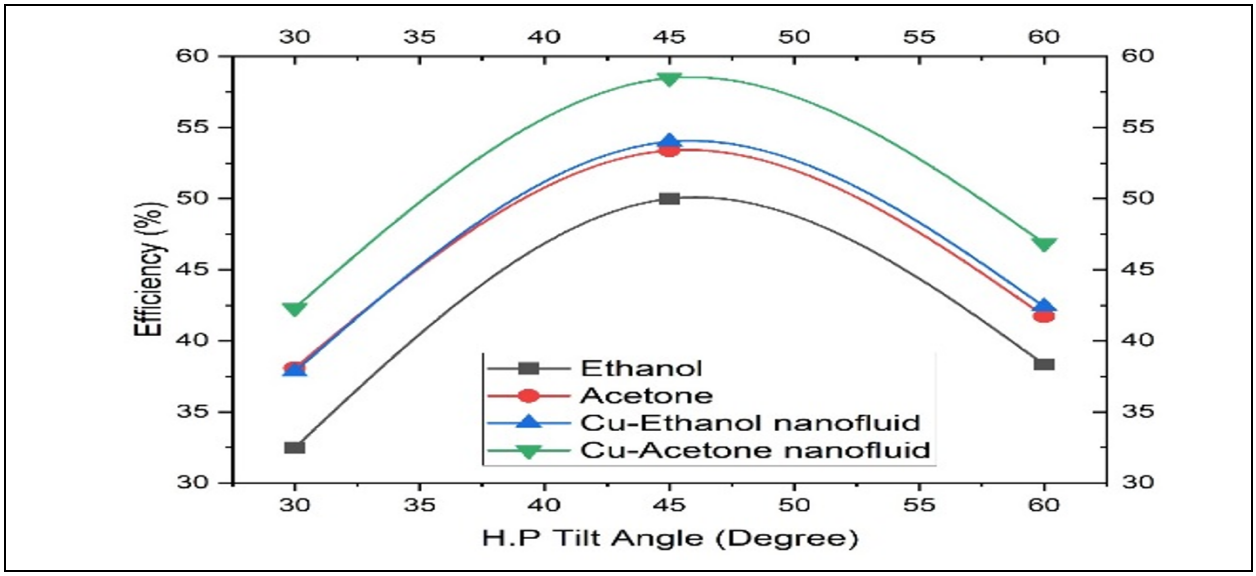


Fig. 15: Heat pipe tilt angle *vs.* efficiency plot for 100 mL of base fluids

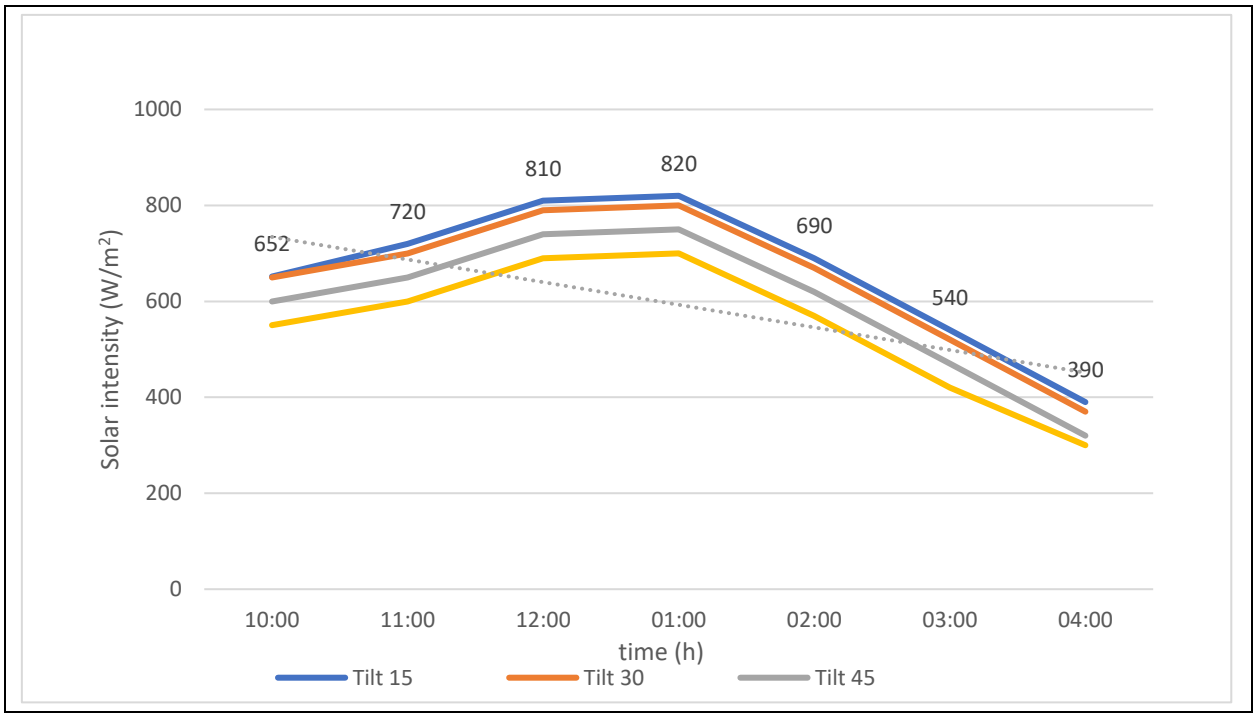


Fig. 16: Solar intensity *vs.* time at different tilt angles

5. CONCLUSION

With a long evaporator area of the heat pipe, the thermal efficiency of the heat pipe has been seen to increase. In the case of an acetone-filled wickless heat pipe, the thermal efficiency has been high compared to the thermal efficiency of ethanol. With the increase in working temperature of the evaporator side of the heat pipe, the overall thermal resistance has increased. Heat pipe efficiency is optimum at a 45° tilt angle. The nanofluid exhibits a higher thermal conductivity ratio, which increases with temperature; consequently, improved thermal performance is observed at elevated temperatures. The addition of nanoparticles significantly enhances the heat-transfer capability of the base fluid. The enhancement in thermal conductivity is directly proportional to both the particle weight fraction and the nanofluid temperature. Therefore, increasing the nanoparticle concentration and operating temperature results in a greater rise in thermal conductivity. Additionally, the specific properties of the nanoparticles and base fluid can influence the thermal conductivity

enhancement, and hence, careful selection of materials is important to achieve optimal results. The solar intensity is higher at lower tilt angles measured from the horizontal. Thereafter, the solar intensity decreases significantly. At all tilt angles, the solar intensity reaches its maximum in the afternoon, around 1:00 p.m. At an identical heat input, the thermal efficiency of the wickless heat pipe with a long evaporator section is lower for ethanol than for acetone. As the tilt angle increases, the efficiency rises up to 45°, beyond which it declines. The thermal resistance of the copper-based nanofluid is lower than that of deionized water. With the increase in the tilt angle, the thermal resistance decreases and reaches an optimum at 45° with respect to the horizontal. Thus, a high-intensity parabolic dish solar concentrator integrated with a long-evaporator wickless heat pipe (thermosyphon) is a promising option for advanced solar water-heating applications.

5.1 Future Recommendations

Every research study offers opportunities for further development and extension. System performance can be enhanced through appropriate modifications, improvements, and technological innovations. The performance of the nanofluid-filled heat pipe may be further optimized by examining the influence of key operating parameters, such as the mode of heat input, flow rate of the working fluid, and ambient conditions. In addition, nanofluid stability remains a critical issue; optimization of surfactant concentration is necessary to improve dispersion stability.

NOMENCLATURE

A_c: Surface area of collector (m^2)
C_p: Specific heat capacity (J/kg K)
d: Diameter of the pipe (m)
G: Solar radiation (W/m^2)
K: Thermal conductivity (W/(m K))
L: Length of the pipe (mm)
m: Mass (kg)
m_f: Mass flow rate (kg/s)
Q: Heat gain of the working fluid (W)
T: Temperature (K)
T_a: Environment temperature (K)
V: Velocity (m/s)
ϕ: Volume fraction (%)
η: Thermal efficiency
ρ: Density (kg/m^3)
μ: Viscosity (kg/(m·s))
b_f: Base fluid
n_f: Nanofluid
np: Nanoparticles
CSP: Concentrated solar power
PFC: Parabolic focus concentrator
SWH: Solar water heater

FUNDING

This research received no specific grant from any funding agency in the public, commercial, or not-for-profit sectors.

CONFLICTS OF INTEREST

The authors declare that there is no conflict of interest.

COPYRIGHT

This article is an open-access article distributed under the terms and conditions of the Creative Commons Attribution (CC BY) license (http://creativecommons.org/licenses/by/4.0/).

REFERENCES

Ali, N., Teixeira, J. A. and Addali, A., A review on nanofluids: fabrication, stability, and thermophysical properties, *J. Nanomater.*, 33, 6978130 (2018). https://doi.org/10.1155/2018/6978130

Chen, Y., Wei, W., Kang, S. and Yu, C., Effect of nanofluid on flat heat pipe thermal performance, *24th IEEE SEMI-THERM Symp.,* 24, 16–19 (2008). https://doi.org/10.1109/STHERM.2008.4509359

Choi, S. U. S., Enhancing thermal conductivity of fluids with nanoparticles, *ASME FED*, 231, 99–105 (1995).

Choudhary, R., Khurana, D., Kumar, A. and Subudhi, S., Stability analysis of Al_2O_3/water nanofluids, *J. Exp. Nanosci.,* 12(1), 140-151 (2017). https://doi.org/10.1080/17458080.2017.1285445

Gan, Y. Y., Ong, H. C., Ling, T. C., Zulkifli, N. W. M., Wang, C. T. and Yang, Y. C., Thermal conductivity optimization and entropy generation analysis of titanium dioxide nanofluid in evacuated tube solar collector, *Appl. Therm. Eng.*, 145, 155–164 (2018). https://doi.org/10.1016/j.applthermaleng.2018.09.012

Ghadimi, A., Saidur, R. and Metselaar, H. S. C., A review of nanofluid stability properties and characterization in stationary conditions, *Int. J. Heat Mass Transfer*, 54(18), 4051–4068 (2011). https://doi.org/10.1016/j.ijheatmasstransfer.2011.04.014

Leonard, M. P., Steven, P. B. and Amir, F., Thermal performance of heat pipes using nanofluids, *Int. J. Heat Mass Transfer*, 107, 358-371(2017). https://doi.org/10.1016/j.ijheatmasstransfer.2016.10.111

Mohammad, A. N., Roghayeh, G. and Mohammad, H. A., Review on using nanofluids in heat pipes, *J. Therm. Anal. Calorim.,* 137, 1847–1855 (2019). https://doi.org/10.1007/s10973-019-08094-y

Mohammed, J. A., Ahmed, K. H., Adel, A. E. and Ammar, I. A., A review on application and technique of improving the performance of heat pipe solar collector system, *Sol. Energy,* 236, 417-433 (2022). https://doi.org/10.1016/j.solener.2022.03.022

Pise, G. A., Salve, S. S., Pise, A. T. and Pise, A. A., Investigation of Solar Heat Pipe Collector Using Nanofluid and Surfactant, *Energy Procedia*, 90, 481-491(2016). https://doi.org/10.1016/j.egypro.2016.11.215

Sabiha, M. A., R. Saidur, S., Hassani, Z. S. and Saad, Energy performance of an evacuated tube solar collector using single walled carbon nanotubes nanofluids, *Energy Convers. Manage.*, 105, 1377-1388 (2015). https://doi.org/10.1016/j.enconman.2015.09.009

Shady, M., Henein., Ahmed, A. and Abdel, R., The performance response of a heat pipe evacuated tube solar collector using MgO/MWCNT hybrid nanofluid as a working fluid, *Case Stud. Therm. Eng.,* 33, 101957 (2022). https://doi.org/10.1016/j.csite.2022.101957

Shafahi, M., Bianco, V., Vafai, K. and Manca, O., An investigation of the thermal performance of cylindrical heat pipes using nanofluids*, Int. J. Heat Mass Transfer.,* 53(1–3), 376-383(2010). https://doi.org/10.1016/j.ijheatmasstransfer.2009.09.019

Sinan, Ü., Tayfun, M., Adnan, S. and Hafiz, M. A., Improvement of Heat Pipe Solar Collector Thermal Efficiency Using Al_2O_3/Water and TiO_2/Water Nanofluids*, Int. J. Photoenergy*, 13, 5546508(2021). https://doi.org/10.1155/2021/5546508

Tardy, F. and Sami, S. M., Thermal analysis of heat pipes during thermal storage, *Appl. Therm. Eng*., 29(2-3), 329–333 (2009). https://doi.org/10.1016/j.applthermaleng.2008.02.037

Teng, T. P., Hung, Y. H., Teng, T. C., Mo, H. E. and Hsu, H. G., The effect of alumina/water nanofluid particle size on thermal conductivity, *Appl. Therm. Eng*., 30(14-15), 2213-2218 (2010). https://doi.org/10.1016/j.applthermaleng.2010.05.036

Vand's, B. L., Synthesis and covalent surface modification of carbon nanotubes for preparation of stabilized nanofluid suspensions, *McGill Univers.*, 1-65 (2009).

Xu, R. J., Zhang, X. H., Wang, R. X., Xu, S. H. and Wang, H. S., Experimental investigation of a solar collector integrated with a pulsating heat pipe and a compound parabolic concentrator*, Energy Convers. Manage*., 148, 68-77 (2017). https://doi.org/10.1016/j.enconman.2017.04.045

Xuan, Y. and Li, Q., Heat transfer enhancement of nanofluids, *Int. J. Heat Fluid Flow*., 21(1), 58–64 (2000). https://doi.org/10.1016/S0142-727X(99)00067-3

Yang, X. F., Liu, Z. H. and Zhao, J., Heat transfer performance of a horizontal micro grooved heat pipe using CuO nanofluid*, J. Micro mech. Micro Eng*., 18, 035038 (2008). https://doi.org/ 10.1088/0960-1317/18/3/035038